Sensors & Actuators: B. Chemical 365 (2022) 131906

Contents lists available at ScienceDirect

Sensors and Actuators: B. Chemical

journal homepage: www.elsevier.com/locate/snb

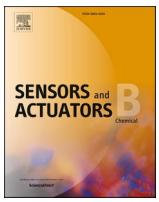

Nanoplasmonic biosensor for rapid detection of multiple viral variants in human serum

Nikhil Bhalla [a,b,*], Amir Farokh Payam [a,b], Alessio Morelli [a], Preetam Kumar Sharma [c], Rhiannon Johnson [d], Alan Thomson [d], Pawan Jolly [e], Francesco Canfarotta [d,**]

[a] Nanotechnology and Integrated Bioengineering Centre (NIBEC), School of Engineering, Ulster University, Jordanstown, Shore Road, Northern Ireland BT37 0QB, United Kingdom
[b] Healthcare Technology Hub, Ulster University, Jordanstown, Shore Road, Northern Ireland BT37 0QB, United Kingdom
[c] Department of Chemical Engineering, Loughborough University, LE11 3TU Loughborough, United Kingdom
[d] MIP Diagnostics, Colworth Park, Sharnbrook, Bedfordshire MK44 1LQ, United Kingdom
[e] Wyss Institute for Biologically Inspired Engineering, Harvard University, CLSB5, 3 Blackfan Circle, Boston, MA 02115, United States

ARTICLE INFO

Keywords:
LSPR
MIPs
Virus
Proteins
Biosensors
Nanoplasmonics

ABSTRACT

As viruses constantly change due to mutation, variants are expected to emerge demanding development of sensors capable of detecting multiple variants using one single sensor platform. Herein, we report the integration of a synthetic binder against SARS-CoV-2 with a nanoplasmonic-based sensing technology, which enables the successful detection of spike proteins of Alpha, Beta and Gamma variants of SARS CoV-2. The recognition event is achieved by specific nanostructured molecularly imprinted polymers (nanoMIPs), developed against a region of the receptor binding domain (RBD) of the SARS CoV-2 spike protein. The transduction is based on the principle of localized surface plasmon resonance (LSPR) associated with silver nanostructures. The nanoMIPs-functionalised LSPR sensor allows for the detection of all 3 protein variants with a limit of detection of 9.71 fM, 7.32 fM and 8.81 pM using wavelength shifts respectively for Alpha, Beta and Gamma spike protein variants. This can be achieved within 30 min from the sample collection, both from blood and using nasal swab, thus making this sensor suitable for rapid detection of COVID-19. Additionally, the turnaround time for sensor development and validation can be completed in less than 8 weeks, making it suitable for addressing future pandemic needs without the requirement for biological binding agents, which is one of the bottlenecks to the supply chain in diagnostic devices.

1. Introduction

With viruses fast evolving into lethal strains, developing new technologies to detect viral infections from a mutated virus at an early stage is a significant challenge [1]. Major strides have been made in understanding viruses from both immunological and biological perspectives, and in particular for SARS CoV-2 in recent times [2]. The new knowledge generated in this active research field has also helped in the validation of advanced fundamental concepts in physical sciences for virus research. For instance, the functional and structural understanding of the spike proteins of SARS CoV-2 and its RNA has led to the development of highly selective and sensitive biosensing technologies to detect the virus [3–6]. These sensors are based on a variety of optical and electronic transduction principles which, in the past, have served as diagnostic platforms for detecting various diseases, with features such as portability, disposability and ease of operation [7].

During the course of the current pandemic, we have witnessed not only a shortage of critical reagents for diagnostics, but also the evolution of new viral variants that demanded for the development of new diagnostic assays capable of detecting multiple variants of the virus. While in

* Corresponding author at: Nanotechnology and Integrated Bioengineering Centre (NIBEC), School of Engineering, Ulster University, Jordanstown, Shore Road, Northern Ireland BT37 0QB, United Kingdom.
** Corresponding author.
E-mail addresses: n.bhalla@ulster.ac.uk (N. Bhalla), a.farokh-payam@ulster.ac.uk (A.F. Payam), a.morelli@ulster.ac.uk (A. Morelli), P.Sharma@lboro.ac.uk (P.K. Sharma), rhiannon.johnson@mip-dx.com (R. Johnson), alan.thomson@mip-dx.com (A. Thomson), pawan.jolly@wyss.harvard.edu (P. Jolly), Francesco.Canfarotta@mip-dx.com (F. Canfarotta).

https://doi.org/10.1016/j.snb.2022.131906
Received 27 February 2022; Received in revised form 12 April 2022; Accepted 13 April 2022
Available online 18 April 2022
0925-4005/© 2022 The Author(s). Published by Elsevier B.V. This is an open access article under the CC BY license (http://creativecommons.org/licenses/by/4.0/).

principle several advanced sensors such as surface plasmon resonance techniques [8], quartz crystal micro balance [9], and electrochemical [10,11] techniques were available for detecting current viruses, the initial diagnostic method of choice, which is also the current gold-standard, was reverse transcription polymerase chain reaction (RT-PCR) [12]. This is mainly due to the fact that RT-PCR generally allows direct and accurate detection of small amounts of genetic material from the virus. However, RT-PCR is prone to false positive/negative (patient history dependent [13,14]) as also seen in our clinical study [15,16] and this issue gets amplified when the virus starts to evolve, requiring new time-consuming genetic studies and templates for upgrading the existing RT-PCR tests.

Therefore, as the time progressed, a cheaper, faster and more accessible method of diagnosis was required, and COVID-19 rapid tests soon became part of everyday life, such as the lateral flow assay tests [17,18]. The latter are based on the direct antigen detection principle and have evolved to be a cost-effective method [19]. Most of the antigen detection is essentially based on antibodies [20]. Whilst antibodies remain the molecular recognition workhorse of choice for bio-sensing devices, their use can impose limitations on widespread technology adoption due to rapidly mutating viral proteins [21]. Issues such as cost, availability, and development time must be taken into consideration when designing a diagnostic device. Typically, developing a new diagnostic device takes longer than for a given virus to mutate, thereby decreasing the sensitivity of the antibody-based assay. One long-championed 'alternative' to antibodies has been molecular imprinting [22,23]; despite few reported applications for viral antigen detection, the approach has had little impact due to limited capability so far [24]. Current published works utilize the use of on-chip polymerization methods which are challenging to scale up into sensing technologies capable of addressing pandemic needs. Therefore, there is a pressing need to develop new technologies that could be quickly implemented and integrated into sensors in order to detect a range of viral antigens, especially if the virus rapidly mutates and may need new binding agent [25].

In order to address the aforementioned challenges, we have used a newly developed synthetic binder against SARS-CoV-2 based on the molecular imprinting technology, which was then integrated in a silver nanoparticle (AgNP) based localized surface plasmon resonance (LSPR) sensor. In particular, the recognition event is accomplished by nanostructured molecularly imprinted polymers (nanoMIPs), developed against a region of the receptor binding domain (RBD). The RBD is a part of the spike protein that binds to a specific endogenous receptor sequence - the Angiotensin-converting enzyme 2 (ACE2) - in order to gain entry into the host cells [26,27]. Hence, developing specific receptors to detect RBD portions (conserved across all variants so far) of the spike would facilitate in the detection of multiple infectious strains of a given virus.

Traditionally, MIPs are produced by polymerizing monomers in the presence of a template molecule (which very often is the target analyte or part thereof). Monomers self- assemble based on the interactions of their functional groups with those present on the target molecule. After polymerization, the target molecule is removed from the polymer matrix, leaving behind imprinted binding sites specific for the size, shape, and functionalities of the target. As receptors, nanoMIPs have experienced a rise in popularity due to their quick development time, control over their surface chemistry, high affinity and robustness. These properties have resulted in MIPs being utilized for various sensing applications such as detection of medical biomarkers, antibiotics, microorganisms, toxins and viruses. However, MIPs tend to suffer from heterogeneous binding affinity, template leaching and slow binding kinetics (particularly in the case of proteins).

In this work, we employed a solid-phase approach for manufacturing nanoMIPs which allows to overcome these problems. Indeed, due to the fact the template molecule is covalently bound to a solid-support, the resulting solid-phase imprinted nanoMIPs possess a more homogenius distribution of binding site affinities and template leaching is therefore avoided. The template used in this work was rationally designed by analyzing in silico the conformation of the RBD domain, looking for the most exposed regions. Three epitopes were identified and produced. Following nanoMIP development, one peptide (around 10 amino acids) of the RBD revealed to be the ideal candidate in generating high affinity nanoMIPs specific for the spike protein. The use of short peptide sequences (instead of the whole RBD or spike protein) allows for reduction in reagent costs and enables the formation of high affinity binding sites for a specific region of the target protein, therefore enhancing the "monoclonality" of the nanoMIPs.

The architecture of our LSPR sensing scheme utilizes silver nanoparticles (AgNP) on glass substrates (Fig. 1a). This LSPR chip is derivatised with nanoMIPs via drop-casting method (Fig. 1b). The size distribution of the AgNPs on the glass substrates showed an average diameter of 22.47 nm (Fig. 1c), with an aspect ratio (ratio of major to minor axis of the particle — where 1 denotes perfect circle) of 1.15. The average spacing between the particles was found to be 26.67 nm. The Alpha, Beta and Gamma variants of the SARS CoV-2 were detected in both blood serum and buffer solution (Fig. 1d-f). The possibility to use either nasal swabs or whole blood using a single measurement technique further highlights the advantage of the current system.

2. Results and discussion

As mentioned above, three epitopes were selected by in silico rational design. Details related to composition and preparation steps are shared in the supporting material and brief summary of fabrication steps is reported in Fig. 1g. Following their production, nanoMIPs were subject to dialysis against DI water in order to remove any potential contaminants collected with the hot fraction. Afterward, the nanoMIPs were analyzed using NanoSight in DI water at room temperature (22.8 °C). As reported in supporting information, the analysis revealed an average size of 69 nm (mode peak at 58 nm), also see Fig. 1h. SPR analysis revealed an apparent KD of 6.5 nM, indicating the developed binders possess high affinity, suitable for sensor implementation. The nanoMIPs used in this work are commercially available and can be purchased from MIP Diagnostics (product number: N108-SC2S-F6AU).

Utilizing atomic force microscopy (AFM), the bare LSPR substrate (Ag), Ag-MIPs and Ag-MIPs-protein substrates were investigated to ascertain their topography (Fig. 2a-c). We found that the LSPR substrate had a uniform distribution of AgNPs over the surface (Fig. 2a), with particle heights ranging from 5 nm to 20 nm and diameters varying from 5 nm to 30 nm (after tip deconvolution) (Fig. 2d). Similarly, we analyzed Ag-MIPs complexes without (Fig. 2b and e, for topography and height analysis respectively) and with protein (Fig. 2c and f, for topography and height analysis respectively). The nanoparticle distribution on the Ag surface and their respective diameters, calculated from the AFM, revealed similar values to those shown by SEM analysis in Fig. 1c. The nanoMIPs deposited over the LSPR substrate form a non-continuous layer (Fig. 2b), with thickness ranging from 20 nm to 40 nm. It should also be noted that it is quite challenging to distinguish between Ag-MIPs without and with protein simply based on their topography, and therefore we show phase differences between these conditions on the Ag surfaces. In Fig. 2, we observe the phase for bare Ag chip which can easily be distinguished from the phase of the Ag-MIPs complex without protein (Fig. 2). Our qualitative analysis show that the MIPs surface becomes softer upon attachment of the proteins as revealed by the tip/surface interaction of the AFM measurement [28]. We have avoided detailed interfacial analysis of the Ag/MIPs/protein interactions using AFM as we wish to focus on the detection performance of the nanoMIPs using the developed LSPR sensor. Nevertheless, our AFM results provide evidence, in addition to SEM, that nanoMIPs were successfully attached on the silver surface.

After confirming the presence of the nanoMIPs on the sensor surface, we evaluated their LSPR performance by detecting spike proteins of

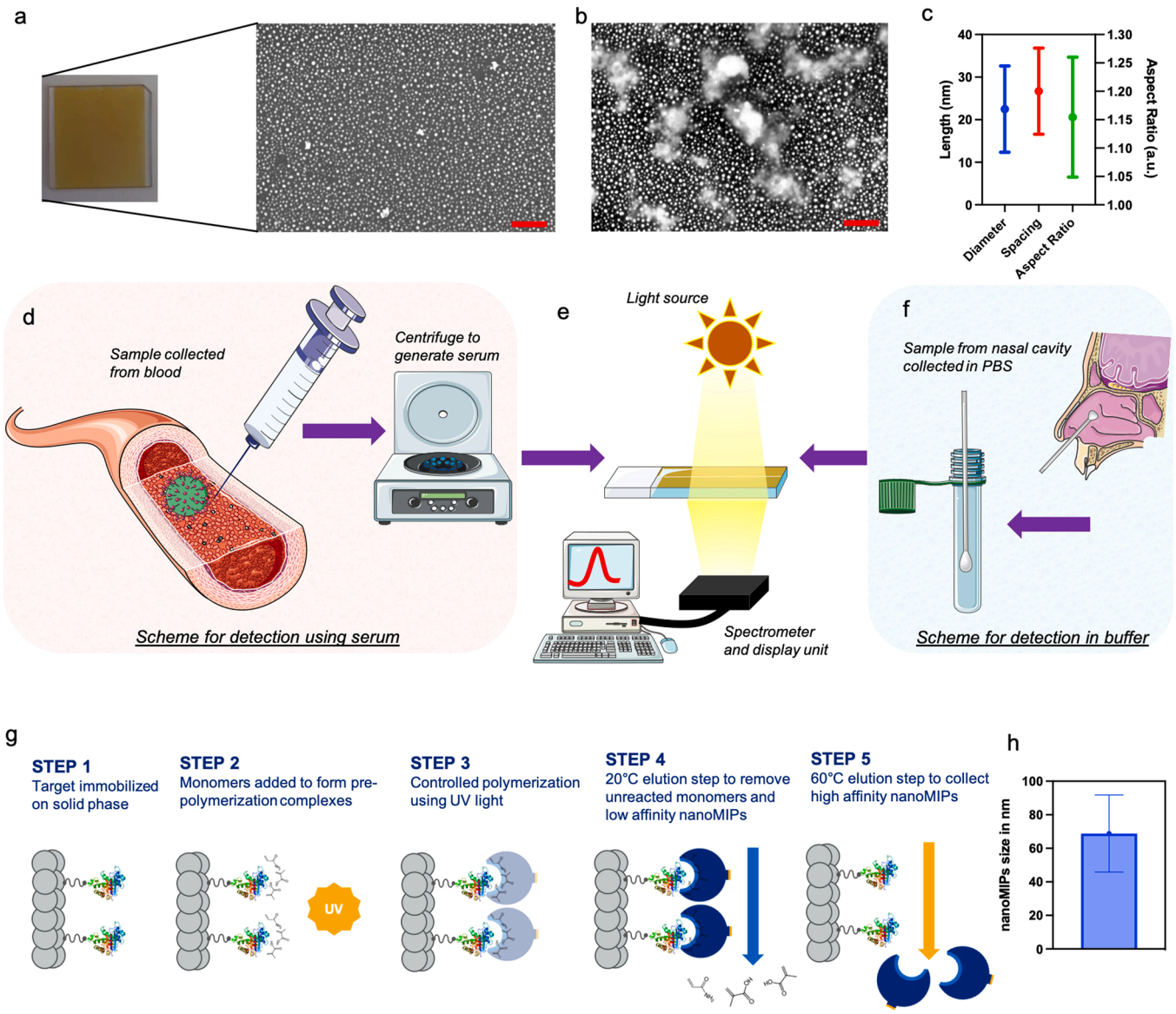

Fig. 1. Sensor architecture and sensing scheme: a) LSPR silver chip and SEM image of its top surface; b) SEM image showing LSPR chip surface immobilized with nanoMIPs. Note that in both a) and b), the red scale bar indicated 500 nm. The image is acquired at 10 kV with a 35,000 X magnification; c) diameter, spacing and aspect ratio of the Ag nanostructures on the LSPR chip; d) schematic showing blood sample collection with a centrifuge to generate serum; e) shows the LSPR measurement with light source and spectrometer; f) depicts the sample collection from nasal cavity to buffer. Both d) and f) point towards the measurement setup in e) indicating that the chip is suitable for detection of analyte collected in buffer by swabs or directly from the blood; g) steps in nanoMIPs development; h) shows the size of nanoMIPs measured using NanoSight particle analyzer.

Alpha, Beta and Gamma variants of the SARS-CoV-2 virus (hereafter referred to as Alpha, Beta and Gamma) in phosphate buffer saline (PBS).

As reported in Fig. 3, the sensor demonstrated successful detection of Alpha, Beta and Gamma. Fig. 3a shows a typical LSPR sensor response upon binding of various concentrations of protein together with the corresponding absorbances. Note that the absorbance shifts here refer to the total area under the LSPR curve obtained for a given concentration. From the obtained results, various trends in wavelength and absorbance are observed. For instance, the wavelength shifts for Alpha and Gamma, are found to have logistic response in comparison to a linear response in the case of Beta, Fig. 3b. The limit of detection (LOD) using wavelength data was found at 466.37 nm, 467.13 nm and 467.71 nm which corresponds to 9.71 fM, 7.32 fM and 8.81 pM respectively for Alpha, Beta and Gamma. The LOD was computed using empirical formula involving the use of limit of blank (LOB) and standard deviations of the measurements, where blank refers to the effect of PBS on the MIPs (without any proteins); further details are reported in the supporting information file.

The absorbance shifts, on the other hand, show no typical dose-response see supporting information for more details. However, one can clearly observe the difference in absorbance obtained from the controls performed using spike proteins of human coronaviruses (HCoV-OC43, HKU1 and HCoV-229E) above 10 fM concentrations of Alpha and Beta, and 100 pM of Gamma, which are represented by the dotted line figures within supporting information. Nevertheless, we can still use absorbance data to indicate the presence of any of the 3 proteins above the concentration of 100 pM and therefore the absorbance data can still be used to develop 'on-off' type sensor, where the presence of any spike protein above 100 pM can be considered as 'on state' and anything below 100 pM, the sensor will be considered as the 'off- state'. We have summarized these wavelengths and absorbance measurements by plotting heat maps to compare all controls, including the blank PBS sample (called buffer) and dose- response for NIPS (non-imprinted polymers) in Fig. 3c, d. The heat maps show a pictorial representation of the LOD and the threshold of 'on-state' discussed above, allowing the user to visualize

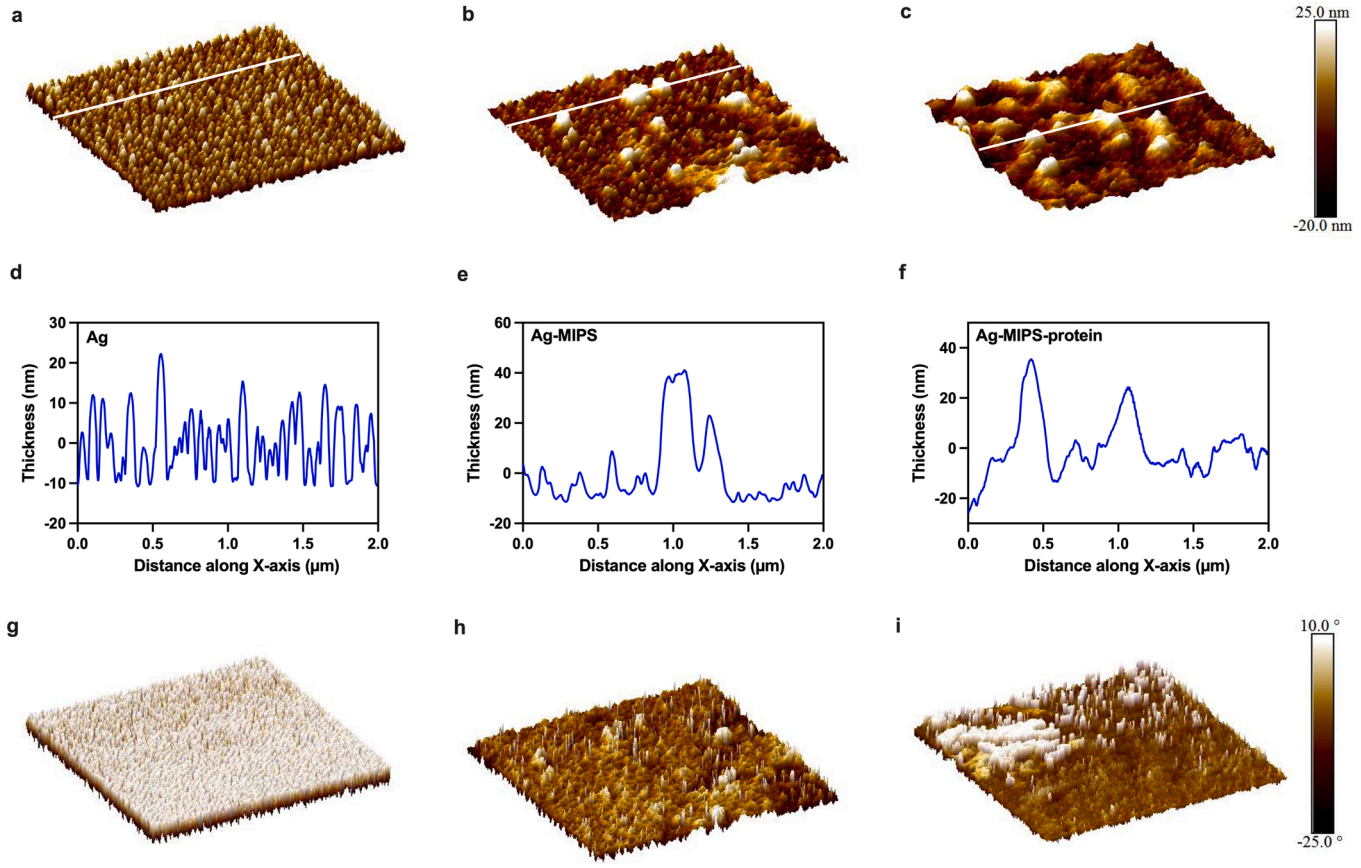

Fig. 2. Atomic force microscopy analysis: a), b), c) show the topography of the Ag, Ag-MIPs and Ag-MIPs with spike protein of Alpha variant of SARS CoV-2 respectively; d), e), f) correspond to the height of the line scans shown in the subfigure a), b) and c) respectively; g), h) and i) show the phase differences observed in the surfaces of Ag, Ag-MIPs and Ag-MIPs with spike protein of Alpha variant of SARS CoV-2 respectively.

the distinction between controls and samples. The heat map data could also potentially be used to encourage implementation of machine learning in the measurement system, developing automatic 'on-off' type of sensors for rapid detection of the analyte above a certain (clinically relevant) concentration.

Following the successful detection of virus samples in PBS, we extended our experiments to clinically relevant fluids by evaluating the performance of the sensor in human serum. In particular, serum was spiked with 100 fM, 10 pM, 1 nM and 100 nM concentrations of Alpha, Beta and Gamma and wavelength and absorbance shifts were measured as shown in Fig. 4. Control experiments were also conducted with human coronavirus proteins at a concentration of 100 nM. Fig. 4a shows a typical LSPR sensor response to blood serum spiked with various concentrations of the Alpha. Alpha and Beta revealed logistic and linear trends in the data as shown in the Fig. 4b. The LOD computed for Alpha and Beta using wavelength data was found to be at 457.54 nm and 460.49 nm. These LOD values correspond to concentrations of 14 fM for Alpha and 94 fM for Beta. The calculated LOD was 130 fM (at 457.37 nm) for wavelength changes observed for Gamma binding, as also shown in Fig. 4b. Note that for LOB calculation, necessary for computing LOD, measurements in serum without protein were considered as blank samples, (see details in the supporting information file). These LOD values were lower than the wavelength shifts measured from the controls (with human coronavirus). We attribute this to low wavelength shifts measured for the blank samples (blank sample measurement is required for LOD calculation). Therefore, the LOD here should be considered only as a mathematical value obtained using the empirical formula of LOD. In such scenarios, a more relevant sensor parameter is the limit of quantification (LOQ)— referred to as the lowest concentration at which the analyte can be reliably detected whereby some predefined goals for bias are also met. In our case if we consider values which can be distinguished from the controls as a bias for LOQ, we can clearly see that the concentration of 10 pM can easily be distinguished from the controls and therefore we can consider 10 pM as LOQ of our sensor in serum based on wavelength shifts.

Similarly, for absorbance shifts, even though we do not observe a specific dose-response trend, the controls can easily be distinguished from the concentration of 10 pM in all 3 protein samples tested (see supporting information) which further suggests that the developed LSPR sensor can reliably detect spike proteins in human serum at a concentration of 10 pM. To visualize our analyses, we plot heat maps to reveal differences between controls and the experiment of interest for both wavelength shifts (Fig. 4c) and absorbance shifts (Fig. 4d) of the LSPR sensor including dose-response for NIPS.

Furthermore, we compared all LSPR data acquired from the protein in buffer (PBS) with those achieved in serum as reported in Fig. 5a-e. We then performed a Šídák multiple comparison (which assumes that each comparison is independent from the others) test using 2-way ANOVA method built within Graphpad prism. For Alpha, Fig. 5a, significant differences between buffer and serum are only observed at higher concentrations (at 100 nM) where large standard deviations are observed within the tests conducted in the buffer. For Beta, Fig. 5b no significant differences are observed in our statistical analysis and for Gamma, Fig. 5c we observe statistical difference only at 10 nM. These differences are attributed to the changes in the differences in blank serum as seen from Fig. 5d. Perhaps non-specific attachment from the other proteins in the serum may lead to some differences in the buffer and serum measurement values. However, it should be noted that the non-specific binding is insignificant since our experiments can be distinguished from the controls carried out using human coronaviruses and blank

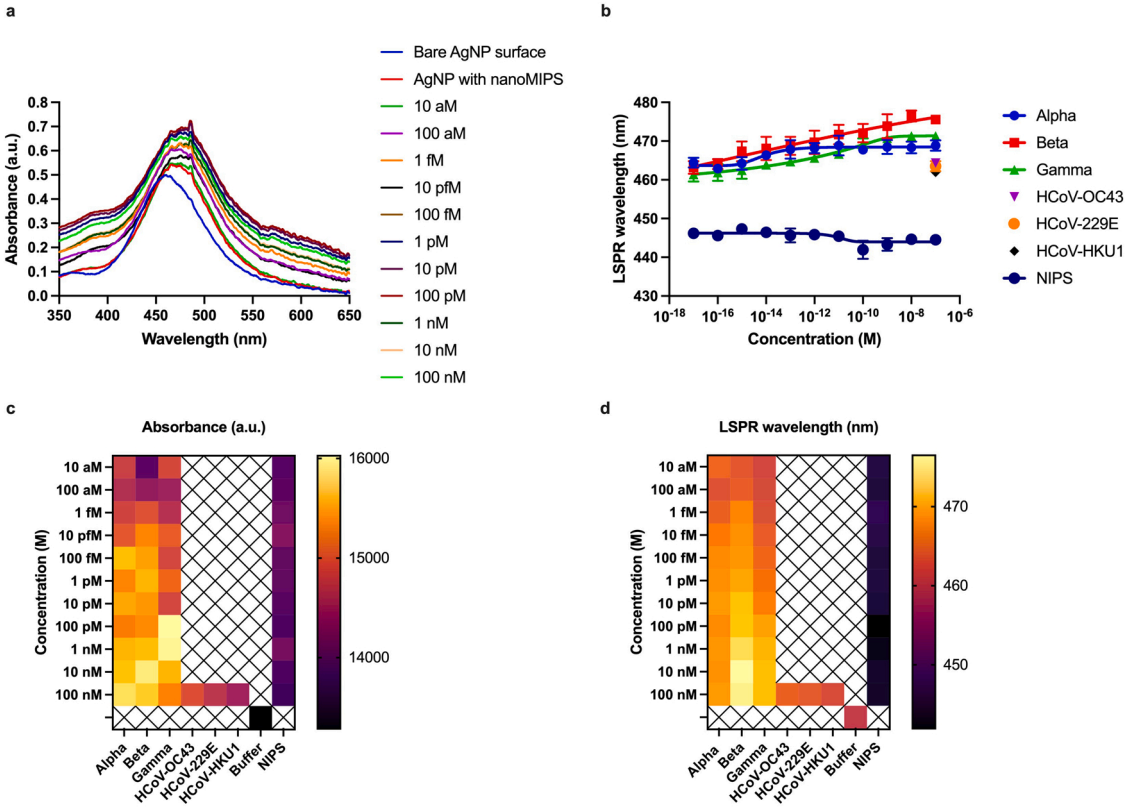

Fig. 3. LSPR detection of spike proteins in PBS: a) LSPR spectrum in wavelength vs absorbance plot for concentrations ranging from 10 aM to 100 nM of the Alpha variant of SARS CoV-2. b) change in LSPR wavelength of the Ag-MIPs complex upon varying the concentration of Alpha, Beta and Gamma from 10 aM to 100 nM. Note that it also shows the controls performed using human coronavirus spike proteins. c) and d) show the heat map comparing LSPR wavelength and absorbance for all concentrations of tested spike proteins, controls with human coronavirus and blank buffer.

buffer/serum. To further assess the buffer and serum experiments, we compared all measurements conducted for individual concentrations in buffer, serum and control experiments (Fig. 5e). We observed a quasi linear trend between the values of serum and buffer. We use the term quasi linear because linear regression showed a low regression coefficient (0.89) within confidence level of 95%. Nevertheless, the comparison still reveals a similar trend between the LSPR measurements acquired in buffer and serum samples. A possible algorithm which considers offsets between 2 different sets of data can potentially be used to compare these measurements which would allow the user to input buffer or serum during the measurement in a given display unit. We also performed stability tests of the AgNP-MIPs surface to evaluate the shelf life of the developed sensor. As shown in Fig. 5 f, we observed a blueshift from 462.31 to 461.92 over 30 days, which is less than 0.5% in the resonance characteristics of the Ag chip. With such minute differences in wavelength, we consider our fictionalized chip to be stable over a period of 30 days.

3. Conclusion

Herein, we described the development of a new synthetic binder based on the molecular imprinting technology specific for the Spike protein of the SARS-CoV-2 virus, and its successful integration into an LSPR sensor for a rapid detection of COVID variants. Molecularly imprinted nanoparticles (nanoMIPs) were developed against an epitope of the RBD region, showing high affinity (KD at 6.5 nM) and selectivity towards the Spike protein. Exploiting the high affinity and selectivity of these synthetic binders, our sensor platform demonstrated to be capable of detecting multiple variants of the SARS CoV-2 virus. Such proof of concept was achieved both in buffer and serum, with the developed sensor being able to distinguish between SARS CoV-2 and other human coronaviruses. Additionally, the LSPR substrate is cost effective (can be mass-produced at a price of less than £0.10), disposable, and compatible with portable readouts for LSPR. Furthermore, compared to antibodies our sensor showed a relatively long shelf life, thanks also to the intrinsic robustness of the integrated nanoMIPs. It is worth highlighting that the development and validation of the sensor system reported here was achieved in less than 8 weeks. The rapid turnaround time makes our technology ideal for those scenarios in which new binders or sensors are required to be developed promptly, such as when new variants or strains emerge. The ease of use and short analysis time of our sensor can also be potentially beneficial in implementing Track and Trace systems during pandemics [29]. The LSPR sensor described in this work represents an important innovation in the field of point of care for viral strain detection and can potentially help keeping epidemics under control if testing is carried out at an early stage.

4. Methods

4.1. Materials

All buffer solutions were prepared using deionized (DI) water (18.2 MΩ), and chemicals were used as purchased, unless specified. nanoMIPs were purchased from MIP Diagnostics, product number: N108-SC2S-F6AU. The peptide used as template to generate nanoMIPs was purchased from Ontores Biotechnology (China). Monomers for the nanoMIP synthesis, sodium hydroxyde, (3-Aminopropyl)triethoxysilane, 1-ethyl-3-(3-dimethylaminopropyl) carbodiimide (EDC), N-hydroxysuccinimide (NHS) were purchased from Merck (UK). All proteins were purchased from antibodies-online.com: Alpha, SARS-CoV-2 Spike protein lineage B.1.1.7, product number: ABIN6963738; Beta, SARS-CoV-2 Spike protein lineage B.1.351, product number:

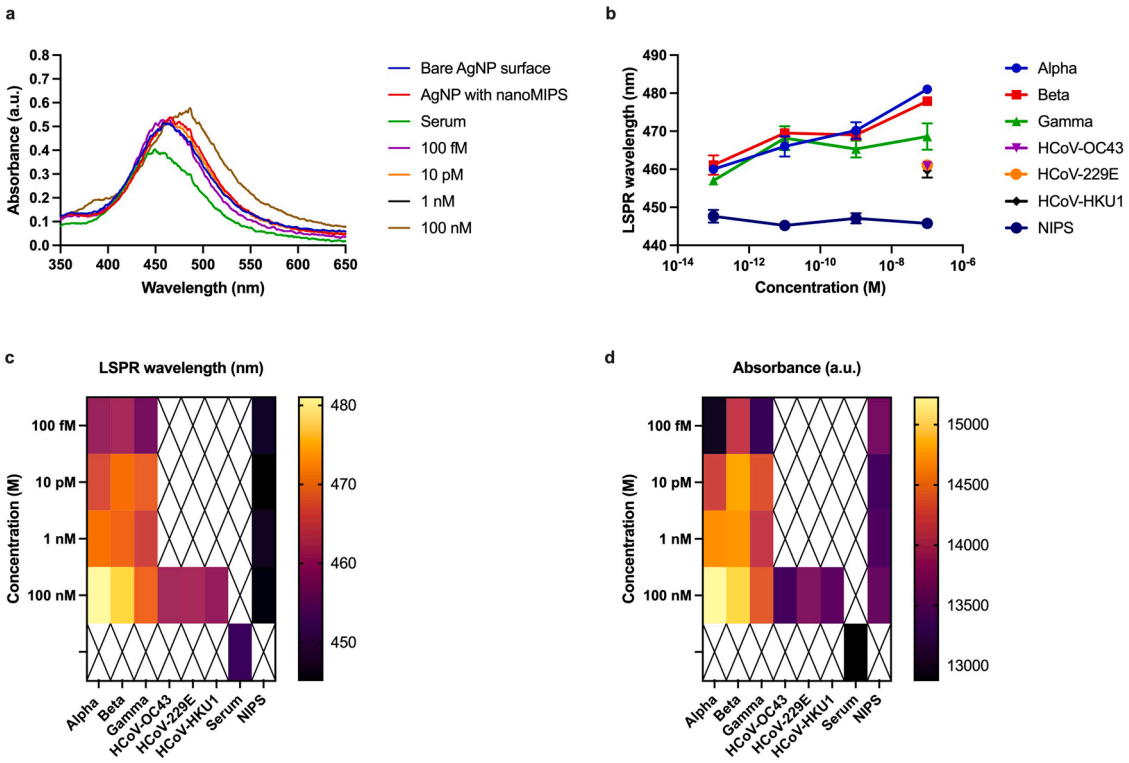

Fig. 4. LSPR detection of spike proteins in serum: a) LSPR spectrum in wavelength vs absorbance plot for concentrations ranging from 100 fM to 100 nM for Alpha variant of SARS CoV-2; b) change in LSPR wavelength of the Ag-MIPs complex upon varying the concentration of Alpha, Beta and Gamma from 100 fM to 100 nM. Note that we also show the controls performed using human coronavirus spike proteins. c) and d) show the heat map comparing LSPR wavelength and absorbance for all concentrations of the tested spike proteins, controls with human coronavirus and blood serum.

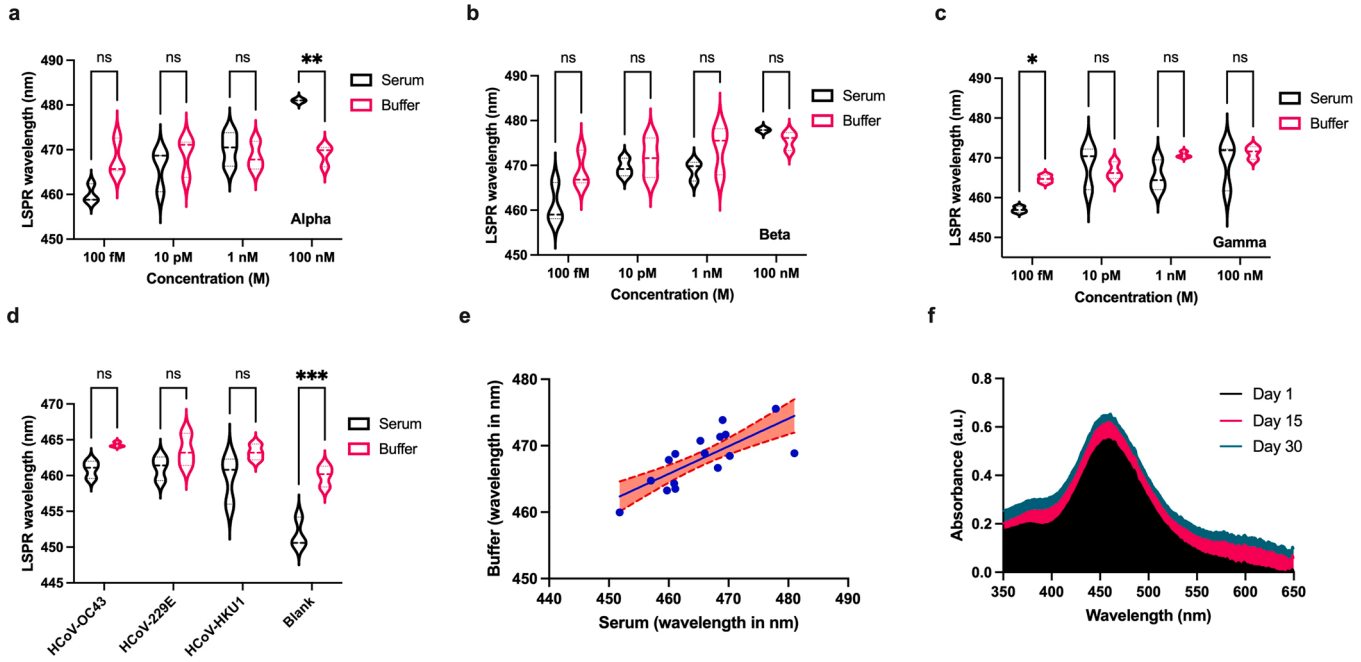

Fig. 5. Sensor analysis: a), b), c) show performance comparison of the developed LSPR sensor (wavelength shifts) for Alpha, Beta, Gamma variants of SARS CoV-2 virus; d) shows comparison of controls including effect of buffer and serum on the sensor surface. The statistical analysis is performed using 2way ANOVA multiple comparisons using Šídák multiple method where Alpha value is 0.05 for the test. Note that 'ns' indicates that data is not significant and '*' denotes the significant level for $p < 0.05$; e) shows the comparison between the buffer and serum measurements where each dot indicates mean values of multiple measurements for a given concentration. The line is fitted with a linear regression (Buffer $= 0.4150 \times$ Serum $+ 274.9$, R squared value of 0.89). The interval, shown in the shaded region indicates confidence level of 95%; f) shows the stability of the Ag-MIPS complex over a period of 30 days with LSPR spectrum of day 1, day 15 and day 30.

ABIN6963739; Gamma, SARS-CoV-2 Spike protein lineage P.1, product number: ABIN6964442; Coronavirus OC43 Spike protein (HCoV-OC43 S), product number: ABIN4976647; Coronavirus HCoV-229E S1 protein, product number: sin-v52h4; Coronavirus HCoV-HKU1 S1 protein, product number: sin-v52h6. Ag chips were purchased from NanoSPR devices, USA, product number: BA3220. CRP free blood serum was purchased from Fitzgerald, product number 90R-100, batch number S18050417.

4.2. nanoMIPs production

The synthesis method was adapted from Canfarotta et al. [30] and it relies on the immobilization of the target peptide on a solid support (glass beads with a diameter between 70 and 100 micrometers). This is accomplished by activating such glass beads with sodium hydroxide (4 M) and then functionalizing them with an amino-silane to obtain primary amine groups on their surface. Epitopes of the RBD region were identified by in silico analysis. These epitopes were then produced and immobilized onto the amine-derivatized glass beads via succinimidyl-iodoacetate coupling. Immobilization of the peptide was confirmed by monitoring color changes with a bicinchoninic acid assay. Polymerization was then initiated by ammonium persulfate (Fig. S1). After polymerization (1 h), the solid support was used to isolate high affinity nanoMIPs from the remaining monomers, oligomers, and low-affinity polymers. This was achieved via a low temperature elution (20 °C), followed by an elevated temperature elution step (60 °C).

4.3. Sensor fabrication

50 μl of a nanoMIP stock solution (5 μg/ml in DI water) was dispensed on the Ag-LSPR chips. Afterwards, the Ag chips were placed inside a humidified chamber for 3 h to ensure that the nanoMIPs were immobilized on the surface of the Ag nanoparticles. Since the nanoMIPs bear amine groups, electrostatic interactions between the negative LSPR Ag surface and the positively charged nanoMIPs (-Ag with NH3 +)resulted in binding of the nanoMIPs to the surface [31]. After this the Ag substrates were thoroughly rinsed with DI water to remove any loosely-bound polymers from the electrode surface. The chips were the stored at 4 ^{o}C until further use. Note that we found that the developed Ag-MIPs chips could be reliably used for 30 days without loss in performance.

4.4. Scanning electron microscopy analysis

The morphology of the Ag LSPR chip-with and without nanoMIPs was characterized with a field emission scanning electron microscope (Hitachi SU5000) in low-vacuum mode using back-scattered electron (BSE) detector at a 10 kV accelerating voltage. Prior to mounting the chip on a circular stub inside the instrument, sputter-coating with a 20 nm palladium film was performed using an Emitech K500X sputtering system in order to avoid electron charging during the imaging process. The image analysis is used to reveal morphological features such as diameter of the particles, their aspect ratio and spacing and it was performed using in-built functions within the ImageJ software.

4.5. Atomic force microscopy analysis

Topographic characterization was performed in air using a commercial atomic force microscope (AFM) system (D3100 Nanoscope III Digital Instruments, now Bruker) in amplitude modulation AFM (tapping mode). Images of 2 μm scan size were acquired with a silicon probe for soft tapping mode (FMV-A Bruker, spring constant 2.8 Nm^{-1}, resonance frequency 78 kHz). Lateral dimensions evaluation was performed by convolution, assuming the nominal radius of curvature (8 nm) is preserved throughout the investigations.

4.6. LSPR data acquisition and analysis

The LSPR signal was acquired using setups used in our previous works [32]. This is a home made setup which consists of components purchased from Ocean Optics: spectrometer FLAME-T-XR1-ES, reflection probe QR400-7-SR-BX, UV-Vis patch connectors, DH-2000 Deuterium-Tungsten Halogen lamp (DH 2000-S-DUV-TTL), RTL-T stage, and Ocean View software. Prior to the acquisition of the LSPR spectrum, dark and reference signals for background noise cancellation were measured using glass slide as a reference. This glass slide was the same substrate on which Ag were deposited. We generated this reference substrate by complete removal of Ag nanoparticles from one of the substrates by sonicating the substrate in acetone for 1 hr and then using isopropanol wipes to clean the surfaces. All generated data were analyzed and plotted using the in-built functionality of the GraphPad Prism 9 software. Some figures presenting our schemes to show LSPR setups were drawn by modifying components available in the source smart servier medical art (smart.servier.com**).**

4.7. Bioassay protocol

All spike proteins including those of the human coronavirus used as controls were pre- pared or diluted with PBS/serum at different concentrations according to our range (10 aM to 100 nM). To perform the dose response in the assay, the Ag-MIPs functionalised substrate was exposed to different concentrations of the respective protein. This was done by simply drop-casting 50 μl of the sample on the Ag-MIPs. After exposing the surface of the sensor to a given concentration, we provided 20 min of incubation time to allow the protein to interact with the MIPs. Thereafter, the surface of the sensor was washed with PBS (for both PBS and serum samples) and then measured the LSPR signal. To acquire the signal, we waited for 30 s during which the ocean view software acquired multiple spectrum and displayed an average of 10 spectrums with a box car width of 5. The LSPR spectra were later saved and wavelength/absorbance shifts were recorded, analyzed and plotted using Graphpad Prism software.

CRediT authorship contribution statement

N.B. designed the research, performed most of the LSPR experiments, analysis, prepared initial and revised manuscript drafts. **A.F.P. and A.M.** performed AFM experiments and analysis. **P.K.S.** performed SEM analysis. **R.J., A.T., F.C.** developed nanoMIPs. **P.J.** provided expertise in integrating nanoMIPs with AgNI surfaces. **N.B. and F.C.** supervised the research. **N.B.** provided all recourses for the study.

Declaration of Competing Interest

The authors declare that they have no known competing financial interests or personal relationships that could have appeared to influence the work reported in this paper.

Appendix A. Supporting information

Supplementary data associated with this article can be found in the online version at doi:10.1016/j.snb.2022.131906.

References

[1] H.C. Ates, A.K. Yetisen, F. Güder, C. Dincer, Wearable devices for the detection of COVID-19, Nat. Electron. 4 (1) (2021) 13–14.
[2] P. V'kovski, A. Kratzel, S. Steiner, H. Stalder, V. Thiel, Coronavirus biology and replication: implica- tions for SARS-CoV-2, Nat. Rev. Microbiol. 19 (3) (2021) 155–170.
[3] F. Narita, Z. Wang, H. Kurita, Z. Li, Y. Shi, Y. Jia, C. Soutis, A review of piezoelectric and magne- tostrictive biosensor materials for detection of COVID-19 and other viruses, Adv. Mater. 33 (1) (2021), 2005448.

[4] P. Fathi-Hafshejani, N. Azam, L. Wang, M.A. Kuroda, M.C. Hamilton, S. Hasim, M. Mahjouri- Samani, Two-dimensional-material-based field-effect transistor biosensor for detecting COVID-19 virus (SARS-CoV-2), ACS nano 15 (7) (2021) 11461–11469.
[5] Z. Song, Y. Ma, M. Chen, A. Ambrosi, C. Ding, X. Luo, Electrochemical biosensor with enhanced antifouling capability for COVID-19 nucleic acid detection in complex biological media, Anal. Chem. 93 (14) (2021) 5963–5971.
[6] R. Funari, K.-Y. Chu, A.Q. Shen, Detection of antibodies against SARS-CoV-2 spike protein by gold nanospikes in an opto-microfluidic chip, Biosens. Bioelectron. 169 (2020), 112578.
[7] M. Mayer, A.J. Baeumner, A megatrend challenging analytical chemistry: biosensor and chemosensor concepts ready for the internet of things, Chem. Rev. 119 (13) (2019) 7996–8027.
[8] N.A.S. Omar, Y.W. Fen, J. Abdullah, Y.M. Kamil, W.M.E.M.M. Daniyal, A. R. Sadrolhos- seini, M.A. Mahdi, Sensitive detection of dengue virus type 2 E-proteins signals using self-assembled monolayers/reduced graphene oxide-PAMAM dendrimer thin film-SPR optical sensor, Sci. Rep. 10 (1) (2020) 1–15.
[9] M.A. Cooper, F.N. Dultsev, T. Minson, V.P. Ostanin, C. Abell, D. Klenerman, Direct and sensitive detection of a human virus by rupture event scanning, Nat. Biotechnol. 19 (9) (2001) 833–837.
[10] F. Patolsky, Y. Weizmann, I. Willner, Redox-active nucleic-acid replica for the amplified bioelectrocat- alytic detection of viral DNA, J. Am. Chem. Soc. 124 (5) (2002) 770–772.
[11] G. Seo, G. Lee, M.J. Kim, S.-H. Baek, M. Choi, K.B. Ku, C.-S. Lee, S. Jun, D. Park, H. G. Kim, Rapid detection of COVID-19 causative virus (SARS-CoV-2) in human nasopharyngeal swab specimens using field-effect transistor-based biosensor, ACS nano 14 (4) (2020) 5135–5142.
[12] I. Smyrlaki, M. Ekman, A. Lentini, N.R. de Sousa, N. Papanicolaou, M. Vondracek, J. Aarum, H. Safari, S. Muradrasoli, A.G. Rothfuchs, Massive and rapid COVID-19 testing is feasible by extraction-free SARS-CoV-2 RT-PCR, Nat. Commun. 11 (1) (2020) 1–12.
[13] M.J. Mina, R. Parker, D.B. Larremore, Rethinking Covid-19 test sensitivity—a strategy for contain- ment, N. Engl. J. Med. 383 (22) (2020), e120.
[14] M.J. Mina, K.G. Andersen, COVID-19 testing: one size does not fit all, Science 371 (6525) (2021) 126–127.
[15] F. Asadi, R. Shahnazari, N. Bhalla, A.F. Payam, Clinical evaluation of SARS-CoV-2 Lung HRCT and RT-PCR Techniques: towards risk factor based diagnosis of infectious diseases, Comput. Struct. Biotechnol. J. 19 (2021) 2699–2707.
[16] J.-B. Lascarrou, G. Colin, A.L. Thuaut, N. Serck, M. Ohana, B. Sauneuf, G. Geri, J.-B. Mesland, G. Ribeyre, C. Hussenet, Predictors of negative first SARS-CoV-2 RT-PCR despite final diagnosis of COVID-19 and association with outcome, Sci. Rep. 11 (1) (2021) 1–7.
[17] F. Krammer, V. Simon, Serology assays to manage COVID-19, Science 368 (6495) (2020) 1060–1061.
[18] R. Weissleder, H. Lee, J. Ko, M.J. Pittet, COVID-19 diagnostics in context, Sci. Transl. Med. 12 (546) (2020).
[19] K.M. Koczula, A. Gallotta, Lateral flow assays, Essays Biochem. 60 (1) (2016) 111–120.
[20] F. Xiang, X. Wang, X. He, Z. Peng, B. Yang, J. Zhang, Q. Zhou, H. Ye, Y. Ma, H. Li, Antibody detection and dynamic characteristics in patients with coronavirus disease 2019, Clin. Infect. Dis. 71 (8) (2020) 1930–1934.
[21] S.A. Kemp, D.A. Collier, R.P. Datir, I.A. Ferreira, S. Gayed, A. Jahun, M. Hosmillo, C. Rees- Spear, P. Mlcochova, I.U. Lumb, SARS-CoV-2 evolution during treatment of chronic infection, Nature 592 (7853) (2021) 277–282.
[22] V. Ratautaite, R. Boguzaite, E. Brazys, A. Ramanaviciene, E. Ciplys, M. Juozapaitis, R. Slibinskas, M. Bechelany, A. Ramanavicius, Molecularly imprinted polypyrrole based sensor for the detection of SARS-CoV-2 spike glycoprotein, Electrochim. Acta 403 (2022), 139581.
[23] D. Balciunas, D. Plausinaitis, V. Ratautaite, A. Ramanaviciene, A. Ramanavicius, Towards elec-trochemical surface plasmon resonance sensor based on the molecularly imprinted polypyrrole for glyphosate sensing, Talanta (2022), 123252.
[24] J.J. BelBruno, Molecularly imprinted polymers, Chem. Rev. 119 (1) (2018) 94–119.
[25] M. Drobysh, A. Ramanaviciene, R. Viter, C.-F. Chen, U. Samukaite-Bubniene, V. Ratautaite, A. Ra- manavicius, Biosensors for the determination of SARS-CoV-2 virus and diagnosis of COVID-19 infection, Int. J. Mol. Sci. 23 (2) (2022) 666.
[26] F. Li, W. Li, M. Farzan, S.C. Harrison, Structure of SARS coronavirus spike receptor-binding domain complexed with receptor, Science 309 (5742) (2005) 1864–1868.
[27] J. Lan, J. Ge, J. Yu, S. Shan, H. Zhou, S. Fan, Q. Zhang, X. Shi, Q. Wang, L. Zhang, Structure of the SARS-CoV-2 spike receptor-binding domain bound to the ACE2 receptor, Nature 581 (7807) (2020) 215–220.
[28] R. García, R. Magerle, R. Perez, Nanoscale compositional mapping with gentle forces, Nat. Mater. 6 (6) (2007) 405–411.
[29] N. Bhalla, Y. Pan, Z. Yang, A.F. Payam, Opportunities and challenges for biosensors and nanoscale analytical tools for pandemics: COVID-19, ACS nano 14 (7) (2020) 7783–7807.
[30] F. Canfarotta, A. Poma, A. Guerreiro, S. Piletsky, Solid-phase synthesis of molecularly imprinted nanoparticles, Nat. Protoc. 11 (3) (2016) 443–455.
[31] S. Agnihotri, S. Mukherji, S. Mukherji, Immobilized silver nanoparticles enhance contact killing and show highest efficacy: elucidation of the mechanism of bactericidal action of silver, Nanoscale 5 (16) (2013) 7328–7340.
[32] S.V. Puttaswamy, G.V. Lubarsky, C. Kelsey, X. Zhang, D. Finlay, J.A. McLaughlin, N. Bhalla, Nanophotonic-carbohydrate lab-on-a-microneedle for rapid detection of human cystatin C in finger- prick blood, ACS nano 14 (9) (2020) 11939–11949.

Nikhil Bhalla is a Lecturer (Assistant Professor) in the School of Engineering, Ulster University-UK.

Amir Farokh Payam is a Lecturer (Assistant Professor) in the School of Engineering, Ulster University-UK.

Alessio Morelli is a Research Associate in the School of Engineering, Ulster University-UK.

Preetam Kumar Sharma is a Research Associate in the Department of Chemical Engineering, Loughborough University-UK.

Rhiannon Johnson is a Senior Scientist at MIP Diagnostics, UK.

Alan Thomson is Chief Scientific Officer of MIP Diagnostics, UK.

Pawan Jolly is Senior Scientist at Wyss Institute for Biologically Inspired Engineering, Harvard University, USA.

Francesco Canfarotta is Head of Chemistry team with MIP Diagnostics, UK.